IEEE Transaction on Control Systems Technology, vol. 8, no. 4, pp. 589-600

Performance Analysis of Cross-Direction Process Control Using Multivariable and Spectral Models

Dimitry Gorinevsky*, Robert Vyse†, and Michael Heaven†

Phone: (408) 864-7569 Fax: (408) 864-7551
Gorinevsky_Dimitry@HTC.Honeywell.com

Abstract

The paper addresses two interrelated problems in cross-directional (CD) control of papermaking processes. The first problem is explaining paper property streaks observed in many CD control installations. The streaks usually correspond to the high-resolution error profile harmonics with wavelength close to twice the actuator spacing. Typically, the streaks of paper weight or moisture are very stable. A question, which often arises, is if the streaks can be compensated by better tuning of the CD controller.

The second, related, problem addressed in this paper is how the achievable high-resolution error profile and its spectrum depend on the CD controller tuning. The paper compares the performances of a mapped controller and an optimal multivariable controller. It also describes spectral characteristics of CD error profile around the Nyquist frequency. Applications of the developed analysis methodology to a paper mill data where weight streaks are a problem are demonstrated.

*Honeywell Technology Center, CA35-5272H, One Results Way, Cupertino, CA 95014
†Honeywell-Measurex Devron, North Vancouver, B.C., Canada V7J 3S4

1 Introduction

This paper considers some problems of cross-directional (CD) control of paper machines. Paper machines produce a continuous web of the paper from a pulp stock. The paper, as it passes through various parts of the machine, undergoes a number of various process changes. As a result of these processes, a paper sheet with desired properties should be produced at the end of the machine. The important paper properties include weight, moisture, thickness, smoothness, and some others; they need to be maintained uniform and as desired in both the machine direction (MD) and cross-direction (CD), i.e., along and across the direction of the paper web motion, respectively. The goal of the CD control is to maintain flat profiles of the paper properties across the web. These profiles are measured by high-resolution scanners installed on the machine and used by the CD control system for feedback. A typical paper machine is illustrated in Figure 1.

The CD control is performed using CD actuators. Each CD actuator includes a set of the identical actuators distributed (usually uniformly) across the sheet. Depending on the application and the actuator type, there can be 20 to 300 individual actuator units in one CD actuator. An example of an important CD actuator is the weight actuator, which adjusts the stock distribution across the machine by changing the opening of different sections of the slice lip extrusion gap on the machine headbox. The CD control technology can be considered as mature, since CD control systems with various levels of complexity and sophistication have been in operation in many different paper mills around world for more that a decade. Irrespective of the machine type, CD actuator type, or control system brand, these systems on some of the machines exhibit certain properties that are undesirable for the paper manufacturer. In particular, in many installations the profile achieved with a CD control system and measured by a scanner exhibits a regular periodic pattern of the paper property variations, which is typically very stable for given installation of the CD controls. The periodic variations of the CD profile physically correspond to streaks lasting along the paper web. The stable streaks in paper weight and thickness are undesirable in paper making, since they are enhanced when the paper is wound on the reel in the end of the paper machine. They are particularly troublesome for the processes where the paper is used as a base stock for subsequent coating. What makes

the streak problem especially intriguing is that the streaks often have periods close to twice the CD actuator spacing.

The streaks have been attributed to hydrodynamic problems of the stock flow in the machine [1, 16, 22], mechanical defects in the equipment [18, 19], control system problems, inadequacy of the CD actuators and other reasons. Also different vendors of CD controls have claimed various advanced control and profile filtering algorithms that presumably should reduce the streaks. The goal of this paper is to present a simple CD control model and analysis that will help to explain the periodic behavior of the CD actuator profile and understand theoretical limits of the achievable CD control performance. In what follows, the analysis is complemented by application examples for real paper machines. In current industry practice, analysis of the paper machine data puts much emphasis on the spectral content of the steady-state CD measurement profile around the spatial Nyquist frequency. The Nyquist frequency for an actuator system corresponds to the $\frac{1}{2}$ actuator frequency (a spatial period of twice the actuator spacing). It is often argued that CD control is possible and should be attempted below and up to the Nyquist frequency and is impossible beyond it. As the analysis of this paper shows, this statement is not completely accurate.

The analysis of this paper is based on a linear model for CD control and uses the assumption that the shape of CD response for each individual actuator is the same across the web. It is acknowledged herein that such a model does not describe practical systems in an absolutely accurate way, yet this is the type of the model which is explicitly or implicitly used in most of theoretical reasoning regarding CD control design and performance analysis. The model with an identical response shape has an adequate accuracy in most practical cases.

The paper employs both matrix analysis and spectral analysis techniques. The matrix analysis automatically takes into account edge effects and allows for accurate simulation. However, matrix analysis tends to be less understandable for field technical personnel and provides less qualitatively transparent results compared to spectral analysis. Frequency domain analysis is a preferred tool, which is widely used in current engineering practice for CD control. At the same time, an accurate frequency domain understanding of many effects related to CD control mapping and actuator spatial frequency response cannot be found in published CD control

literature. The only exception known to the authors is the recent paper [6], which considers issues of CD control bandwidth and optimality closely relate to the topic of this study. In [6] a CD profile of the process is considered as a function of a continuous CD coordinate, while this paper considers a CD profile sampled along the CD coordinate as encountered in practical CD control.

Section 4 of this paper contains a sampled-coordinate version of the optimality results of [6]. By comparing our results and results of [6] one can see that the bandwidth limitations associated with control of discrete and continuous CD profiles differ in a way that is reminiscent of the bandwidth issues for continuous and discrete-time systems. In particular, in case of sampled measurement (as used in industrial systems and studied in this paper) the frequency aliasing phenomena for the measurement have to be taken into account. A study of the aliasing phenomena is a subject of Section 5 of our paper.

Only optimal CD control is considered in [6]. Unlike that, our paper also considers a "mapped" control approach that is predominantly used in the industrial CD control systems. Sections 3, 4, and 5 of this paper analyze performance for such mapped CD controllers by comparing it and relating it to the optimal controller performance. Our paper specifically considers and analyses a practical problem of the CD profile streaks as it is related to the CD control performance. Sections 5 and 6 of the paper provide discussion and real-life examples of the streak problem, which is really important in the industry.

2 Model for CD profile control

Consider an array of n_a uniformly spaced CD actuators and denote by u a profile of the actuator setpoints

$$u = [u_1 \;\; u_2 \;\; \ldots \;\; u_{n_a}]^T \;\; \in \Re^{n_a}, \tag{1}$$

This paper studies a steady state of the CD control system that is achieved by maintaining the actuator setpoints constant. We will assume that the measurement available to the system is represented by a high-resolution CD profile obtained by sampling paper properties at $m = n_a \cdot m_a$ points uniformly spaced in CD, where m_a is a number of high-resolution pro-

file measurements per CD actuator. In most practical cases, $3 \leq m_a \leq 12$. Denote by q a high-resolution profile vector, measured before the CD control is engaged, i.e., for zero actuator setpoints, $u = 0$. Denote by q_d the target high-resolution profile. In most practical cases the target profile is flat, i.e., all components of q_d are equal. Denote by p an initial high-resolution profile error vector

$$p = [p_1 \;\; p_2 \;\; \ldots \;\; p_m]^T \in \Re^m \,, \quad m = n_a m_a \,, \tag{2}$$

Let us further denote by $p_u = q - q_d$ a steady-state variation of the high-resolution profile obtained for the actuator setpoint profile u, and by $e_u = p - p_u$ the residual error of the high-resolution profile. In accordance with the assumptions made above, variations of the actuator setpoints and high-resolution profile are linearly related. Therefore, we can write

$$p_u = \sum_{j=1}^{n_a} u_j g^j, \tag{3}$$

where $g^j \in \Re^m$ are vectors describing shapes of a high-resolution profile response to individual actuators. Equation (3) can be written in the matrix form as

$$p_u = G\,u \,, \tag{4}$$

$$G = [g^1 \;\; \ldots \;\; g^{n_a}] \in \Re^{m,n_a}, \tag{5}$$

where G is the system gain matrix. Columns of the matrix G are the actuator response shapes g^j. As mentioned above, we assume that responses of the actuators are of the same shape and differ only by shift in the CD coordinate, which we will denote by x. Each response g^j is obtained by sampling a continuous response function of the actuator at the scanner sampling coordinates $x = k$. Thus, the components of the response gain vector g^j have the form

$$g^j_k = b(k - \gamma_j), \qquad k = 1, \; \ldots, \; m \,, \tag{6}$$

where γ_j is the center of the response for the actuator k, and $b(x)$ is a continuous response function (the same for all actuators).

Most of the industrial CD controllers in use today are mapped controllers. Such controllers map the high-resolution profile (2) into an actuator-resolution profile, which is called a control

error profile. Each element of the control error profile v is subsequently used to compute moves of a single respective actuator.

$$v = [v_1 \;\; v_2 \;\; \ldots \;\; v_{n_a}]^T \qquad \in \Re^{n_a}\,, \tag{7}$$

In one of the most sophisticated CD control systems on the market, the control error profile (7) is obtained from the high-resolution error profile (2) by performing filtering with a spatial antialiasing window and/or weighted averaging of the high-resolution data across an actuator zone. Both antialiasing and averaging are linear operations, which means that the control error profile (7) is related to the high-resolution error profile (2) by a linear transformation. This linear transformation can be presented in the matrix form as

$$\begin{aligned} v &= C^T e_u\,, \qquad C \in \Re^{m,n_a}, \\ C &= [c^1 \;\; c^2 \;\; \ldots \;\; c^{n_a}], \quad c^j \in \Re^m, \end{aligned} \tag{8}$$

where C is a *mapping matrix* or observation matrix and superscript T denotes matrix transpose. The columns c^j of the mapping matrix C contain weights with which high-resolution measurements are summed up to obtain the control error profile values.

In general, it is possible to implement a mapping window of an arbitrary shape in the CD control system. The mapping window vectors c^j (8) defined by an antialiasing window and averaging across the actuator zone are of the form

$$c^k = [h_{\mathrm{B}} \otimes z^k]_{m_{\mathrm{B}}}, \tag{9}$$

where h_{B} is the antialiasing window of the width $1+2m_{\mathrm{B}}$, $z^k \in \Re^{n_a}$ is the window with elements $\frac{1}{m_a}$ and 0 that defines averaging across the actuator zone, and $[\cdot]_{m_{\mathrm{B}}}$ denotes truncation of the m_{B} elements on the both sides of the convolution profile.

By using (9) and neglecting edge effects, we can present entries of the mapping matrix C in the following general form:

$$c^k_j = h_{k-m_a(j-1)}, \tag{10}$$

where the kernel mapping window h_k is defined for $-m \le k \le m$ and determines the design of the mapping mechanism in the controller. Note that the described mapping method, differs

significantly from the common square-down methods used in other MIMO process control problems such as described in [23, Chapter 8]. Mapping of the measurement error to actuators is a standard practice in industrial CD control systems, e.g. see [17]. This is one reason why published papers on CD control start from considering a square system model, which corresponds to considering the mapped measurements [4, 2, 11, 15, 21, 27].

3 Matrix Analysis

In this section, we perform matrix analysis of the CD control performance limits. Such analysis is based only on the property of linearity of the system and automatically takes into account edge effects. Such analysis is valid even if the response shape varies across the paper sheet. We first consider an optimal, minimum-variance CD controller, then compare the control quality achievable with such controller and with a mapped controller.

The error profile $e_u = p - Gu$ is defined by the initial error profile p and the actuator profile input u which is used to shape the error profile in a desirable way. The high-resolution error profile has $m = n_a m_a$ elements, while the actuator profile input u has only n_a elements. Thus, performance of CD control in compensating high-resolution profile variation is inherently limited.

The optimal actuator profile u_* that minimizes the variation (mean square value) of the error profile can be found by solving the following quadratic optimization problem

$$U_* = \arg\min \|e_u\|^2, \tag{11}$$

where e_u is the error profile and $\|\cdot\|$ denotes the Euclidean norm of a vector.

By substituting $e_u = p - Gu$ into (11) and differentiating with respect to u, we can obtain a solution to (11). The optimal actuator profile input u_* and the high-resolution error profile $e_* = p - Gu_*$ with the minimal achievable variance have the form

$$u_* = (G^T G)^{-1} G^T p\,, \tag{12}$$

$$e_* = \left(I_m - G(G^T G)^{-1} G^T\right) p\,, \tag{13}$$

where I_m in a $m \times m$ unity matrix.

If the matrix $G^T G$ is not invertible, a least-square optimal control input u can be found by using a *regularization* technique [25], by minimizing a *regularized* performance index of the form

$$U_* = \arg\min[\|e_u\|^2 + \rho\|u\|^2], \tag{14}$$

where ρ is a small positive parameter. The regularized problem solution has the form

$$u_* = (\rho I_{n_a} + G^T G)^{-1} G^T p\,, \tag{15}$$

and for small values of ρ is close to (12). We would like to note here that the regularized solution (15) to the non-square multivariable problem (11) has the form similar to the quadratic-optimal multivariable controller solution considered in [3, 5, 12, 13, 24].

A mapped CD controller strives to compensate for the control error profile deviation from zero (7). As a result of this, control error profile is usually kept small and we will assume that $v = 0$. To find the actuator profile input u_M for the mapped controller providing zero control error profile $v = 0$, let us substitute $e_u = p - p_u$ into (8) and use (4) to obtain the high-resolution error profile e_M corresponding to the zero control profile of the mapped controller.

$$u_M = (C^T G)^{-1} C^T p\,, \tag{16}$$

$$e_M = \left(I_m - G(C^T G)^{-1} C^T\right) p\,, \tag{17}$$

Note that the j-th column w_j of the matrix $C^T G$ in (16), (17) can be found as $w^j = C^T g^j$. The vector w_j, therefore, gives a shape of the actuator response visible in the actuator-resolution control error profile. The actuator setpoint profile and the error profile achieved with a mapped controller, in general, differ from the profiles (12), (13) for the minimum-variance controller and would provide an inferior quadratic variance performance. However, a mapped controller can achieve the *same* error as the minimum-variance controller. Given (12), (13), and (16), (17), the following statement regarding optimal performance of a mapped controller can be made:

The optimal performance of a mapped controller can be achieved by using a mapping window shape exactly coinciding with the shape of the CD actuator response.

Using a mapping window coinsiding with the response shape corresponds to squaring down the system (4) by projecting the error on the image subspace of the gain matrix G. Such projection is achieved by right multiplication by G^T and it gets rid of the uncontrollable measurements belonging to the kernel of G.

This use of the projection follows directly from standard control theory results and is obvious mathematically since there are no dynamics in the system. At the same time, the above rigorous definition of how a mapped CD controller can be made optimal does not seem to be generally acknowledged in the CD control literature and practice. Various spatial filtering and mapping schemes have been proposed by some CD control equipment vendors and research organizations with claims of performance improvement. One of the goals of this paper is to communicate the mapped CD control optimality condition clearly and rigorously to people involved in CD control.

4 Frequency Domain Analysis

In comparison to the matrix analysis, frequency domain analysis does not take edge effects into account. At the same time, results of the frequency domain analysis are intuitively more understandable. Fourier analysis of the CD control is somewhat non-standard because the control and high-resolution profiles have different resolutions. Such analysis can be performed by using the multi-rate signal theory [26].

4.1 Spectral model for CD control

Let us derive a frequency domain model of the CD control (4), (6). When deriving this model, one should take into account that the profiles u and p as well as their Fourier transforms have different resolutions. Since there are exactly m_a measurement points per actuator, multi rate signal analysis results are applicable [26].

A discrete Fourier transform (DFT) computed for a profile $p \in \Re^m$ gives a complex 'frequency component' profile $\tilde{p}$ as

$$\tilde{p} = [\tilde{p}_1 \;\; \tilde{p}_2 \;\; \ldots \;\; \tilde{p}_m]^T \;\in C^m\,, \tag{18}$$

$$\tilde{p}_k = \sum_{l=1}^{m} e^{i\omega_{k-1}(l-1)} p_l \,, \qquad \omega_k = \frac{2\pi k}{m}$$

Since the profile p is real-valued, its Fourier transform $\tilde{p}$ possesses certain symmetry properties, in particular in (18)

$$\tilde{p}_k = \tilde{p}^*_{m-k+2} \,, \tag{19}$$

where * denotes complex conjugate. Thus, the power spectrum $|\tilde{p}_k|^2$ is symmetric with respect to the mid-point $m/2+1$.

Consider a DFT of the actuator profile u in (4)

$$\begin{aligned} \tilde{u} &= [\tilde{u}_1 \;\; \tilde{u}_2 \;\; \ldots \;\; \tilde{u}_{n_a}]^T \in C^{n_a} \,, \\ \tilde{u}_n &= \sum_{l=1}^{n_a} e^{i\Omega_{n-1}(l-1)} u_l \,, \qquad \Omega_n = \frac{2\pi n}{n_a} \end{aligned} \tag{20}$$

By using (6), we can present (4) in the form of a convolution of the filter kernel b with the "expanded" [26] signal u.

$$p_{u,j} = \sum_{k=1}^{n_a} g_k^j u_k = \sum_{k=1}^{n_a} b_{k-m_a(j-1)} u_k \tag{21}$$

Let us subdivide the high-resolution profile frequency band into m_a subbands of the length m_a that are multipliers of the actuator profile frequency band in (21).

$$\tilde{p} = \begin{bmatrix} \tilde{p}^1 \\ \vdots \\ \tilde{p}^{m_a} \end{bmatrix} \,, \qquad \tilde{b} = \begin{bmatrix} \tilde{b}^1 \\ \vdots \\ \tilde{b}^{m_a} \end{bmatrix} \,, \qquad \tilde{v} = \begin{bmatrix} \tilde{u} \\ \vdots \\ \tilde{u} \end{bmatrix} \,, \qquad \tilde{p}^j, \tilde{u}, \tilde{b}^j \in C^{n_a} \tag{22}$$

where vector $\tilde{v}$ in (20) consists of m_a stacked images of the Fourier transform $\tilde{u}$.

Note that in accordance with (22),

$$\|\tilde{p}\|^2 = \sum_{j=1}^{m_a} \|\tilde{p}^j\|^2 \tag{23}$$

In accordance with [26, Section 4.1, p. 102],

$$\tilde{p}_{u,n} \equiv \;\; \tilde{b}_n \tilde{v}_n, \tag{24}$$

By using (22), we can write (24) in the form

$$\tilde{p}_u^j = \tilde{b}^j \odot \tilde{u}, \qquad (j = 1, \ldots, m_a), \tag{25}$$

where $\odot$ denotes a component-wise product of two vectors.

The expression (25) shows an aliasing effect in the control of a high-resolution profile with a lower resolution actuator profile. In accordance with (25), each of the actuator profile frequencies influences the high-resolution profile at all of its m_a multipliers. The strength of influence is defined by the spectral content of the actuator shape $\tilde{b}$. Since, normally, the amplitude $|\tilde{b}_k|$ drops sharply with the frequency ω_k, each of the frequency components $\tilde{u}_j$ would visibly influence only a few of the subband profiles $\tilde{p}_j^k$.

From the control design viewpoint, (25) shows that an attempt to control only the low, first-subband, frequencies in the high-resolution profile may cause aliased increase in the higher harmonic amplitude. This effect and the optimal control strategy to overcome it are discussed in the rest of this section.

4.2 Minimum variance solution in the frequency domain

Based on the frequency domain model of the previous subsection, let us find actuator profile input u that will provide for the minimum variance of the residual error profile $e_u = p - p_u$. Similarly to Section 3, we will minimize the performance index of the form (11). By using the Parceval's Identity, the frequency domain model of the CD control (22), (25), and identity (23), we arrive at the following optimization problem, which is equivalent to (11),

$$J = m^{-1}\|\tilde{e}_u\|^2 = m^{-1}\|\tilde{p} - \tilde{p}_u\|^2 = m^{-1}\sum_{j=1}^{m_a}\|\tilde{p}^j - \tilde{b}^j\tilde{u}\|^2 \;\rightarrow\; \min \tag{26}$$

By rewriting (26) in component form, one can see that the contribution of components of $\tilde{u}$ to the performance index can be separated so that the optimum components can be found as

$$\tilde{u}_{*,k} = \arg\min m^{-1}\sum_{k=1}^{n_a}\sum_{j=1}^{m_a}|\tilde{p}_k^j - \tilde{b}_k^j\tilde{u}_k|^2 \tag{27}$$

where $|\cdot|$ denotes an absolute value of a complex number. By solving (27) and substituting $\tilde{u}_{*,k}$ into (25), we obtain

$$\tilde{u}_{*,k} \;=\; \frac{\sum_{j=1}^{m_a}(\tilde{b}_k^j)^*\tilde{p}_k^j}{\sum_{j=1}^{m_a}|\tilde{b}_k^j|^2}, \tag{28}$$

$$\tilde{e}^l_{*,k} \;=\; \frac{\sum_{j=1}^{m_a}(\tilde{b}^j_k)^*(\tilde{b}^j_k\tilde{p}^l_k - \tilde{b}^l_k\tilde{p}^j_k)}{\sum_{j=1}^{m_a}|\tilde{b}^j_k|^2} \tag{29}$$

Since the problem (27) is just a different form of representing (11), the expressions (28), (29) give the same results as (12), (13). Multiplication of the initial profile by the matrix G^T in (12) corresponds to multiplication by $(\tilde{b}^j_k)^*$ and summation over the harmonics in the numerator of (28), while division by the denominator in (28) is the frequency-domain analog of multiplication by the matrix $(G^TG)^{-1}$ in (12).

Before presenting a more detailed analysis of (28), (29), let us consider the case where the denominator of (28) is close to zero. This corresponds to the ill-conditioned matrix $(G^TG)^{-1}$ in (12) and might particularly happen if the spectrum of the actuator response shape $\tilde{b}$ is narrow and goes to zero within the Nyquist frequency range. The narrow spectrum of the actuator response corresponds to the wide physical response of the actuator. It this case one can compute a desirable actuator profile input $\tilde{u}$ by minimizing a regularized performance index of the form (14). In frequency domain, we obtain the following modification of (26) equivalent to (14)

$$J_\rho = m^{-1}\|\tilde{e}_u\|^2 + n_a^{-1}\rho\|\tilde{u}\|^2 = m^{-1}\sum_{k=1}^{n_a}\sum_{j=1}^{m_a}|\tilde{p}^j_k - \tilde{b}^j_k\tilde{u}_k|^2 + \rho|\tilde{u}_k|^2 \;\rightarrow\; \min\,, \tag{30}$$

where ρ is a small positive scalar.

By differentiating (30) to find optimal $\tilde{u}$, we obtain frequency domain equivalent of (15)

$$\tilde{u}_{*,k} = \frac{\sum_{j=1}^{m_a}(\tilde{b}^j_k)^*\tilde{p}^j_k}{m_a\rho + \sum_{j=1}^{m_a}|\tilde{b}^j_k|^2} \tag{31}$$

The regularization is equivalent to adding a small positive value to the denominator of the optimal solution in the frequency domain. This makes the spectral components of the computed actuator profile $\tilde{u}$ bounded even if all of the actuator frequency response harmonics $\tilde{b}^j$ turn into zero at certain frequencies.

Let us note that according to (26), for small (or zero) values of the regularization parameter ρ, the spectral components of the actuator profile $\tilde{u}_k$ can be large at high frequencies, if all actuator response harmonics $\tilde{b}^j_k$ are close to zero. This explains why actuator picketing of large amplitude was observed experimentally in the early attempts to implement optimal control moves based on matrix inversion or multivariable control equivalent to the considered

regularized solution. Picketing of the actuators corresponds to a large amplitude of high-frequency components in the actuator profile. An obvious solution against the picketing is, thus, to increase the penalty parameter ρ in order to achieve a proportional attenuation of these high-frequency components. This solution, however, is not a perfect one, because for large ρ compensation for all spatial frequencies will deteriorate to a certain extent. Methods for avoiding picketing while maintaining a good quality of control are subject of a comprehensive study which is outside of the scope of this paper.

We will perform a frequency-domain study of the least square controller error further in this section together with the analysis of the mapped controller error.

4.3 Frequency domain analysis of a mapped controller

Let us now formulate a frequency domain model of the mapped CD controller. This model will be based on the Section 2 model of the mapped controller observations.

Let us compute a discrete Fourier transform of the control error profile v (8). This profile has the same dimension as the actuator profile u and its Fourier transform can be computed similarly to (20). Note that (8), (10) describe a transformation of the error profile e_k that consists of filtering with the kernel (10) and then m_a-fold "decimation" [26, Section 4.1, p. 102]

$$v_j = \sum_{k=1}^{m} h_{k-m_a(j-1)} e_k \tag{32}$$

In accordance with [26, Section 4.1, p. 102], we obtain from (32) for the Fourier transforms of the signals

$$\tilde{v}_n = \frac{1}{m_a} \sum_{q=1}^{m_a} \tilde{e}_{n+(q-1)n_a} \tilde{h}^*_{n+(q-1)n_a} \tag{33}$$

In the notation of (22), we can re-write (33) in the form

$$\tilde{v} = \frac{1}{m_a} \sum_{q=1}^{m_a} \tilde{e}^q \odot (\tilde{h}^q)^*, \tag{34}$$

where $\odot$ denotes a component-wise product of two vectors.

Expression (33) shows an aliasing effect of the higher harmonics of the sampling frequency on the control error profile. The strength of this aliasing effect is defined by the spectral

characteristics of the mapping window h_k. Current practice in the tuning of the mapped controllers is to shape this window using a spatial smoothing filter in order to get rid of the aliasing effect. We will further show that such filtering may not provide the best possible CD control performance.

Let us find the actuator profile input for the mapped controller that will be achieved if the CD feedback loop is designed in the appropriate way. As already discussed, with this input u_M, the control error profile obtained for the high-resolution error profile should provide for a zero control error profile $v = 0$. By substituting into (33) the error profile $\tilde{e}_u = \tilde{p} - \tilde{p}_u$, where $\tilde{p}_u$ is defined by (21), we obtain that the optimal input u_M of the mapped controller should satisfy

$$0 \quad = \quad \sum_{q=1}^{m_a} (\tilde{h}_k^q)^* (\tilde{p}_k^q - \tilde{b}_k^q \tilde{u}_{M,k}) \tag{35}$$

By formally solving (35), we find the optimal actuator profile input in the form

$$\tilde{u}_{M,k} \quad = \quad \frac{\sum_{q=1}^{m_a} (\tilde{h}_k^q)^* \tilde{p}_k^q}{\sum_{q=1}^{m_a} (\tilde{h}_k^q)^* \tilde{b}_k^q} \tag{36}$$

This expression can potentially give very large values of the actuator profile spectral components (picketing) if the denominator in (35) is close to zero. In particular, this may happen if the actuator response $\tilde{b}$ has a cut-off frequency lower than the Nyquist frequency of the actuator system.

By substituting (36) into (25) and computing the error $\tilde{e}_u = \tilde{p} - \tilde{p}_u$, we obtain frequency domain equivalent of (16), (17)

$$\tilde{e}_{M,k}^n \quad = \quad \frac{\sum_{q=1}^{m_a} (\tilde{h}_k^q)^* (\tilde{p}_k^n \tilde{b}_k^q - \tilde{p}_k^q \tilde{b}_k^n)}{\sum_{q=1}^{m_a} (\tilde{h}_k^q)^* \tilde{b}_k^q} \tag{37}$$

We will study the spectral contents of the control error profile and the error profile of a mapped controller in more detail in the next subsection. Here we would just like to note that the total variation $\|\tilde{e}_u\|^2$ of the error profile for a mapped controller can not be less than the variation (29) for the minimum variance controller (28). By comparing (36) and (28), one can see that the mapped controller will be equivalent to the minimum variance controller if $\tilde{h}_k^q = \text{const}\ \tilde{b}_k^q$, i.e., if the mapping window has the same shape as the actuator response.

5 Study of Aliasing Effects

Let us analyze effects of aliasing on CD control in more detail both for a general mapped and a minimum variance controller. For this analysis, we will assume that the frequency response $\tilde{b}$ of the CD actuator decays fast outside the Nyquist frequency range. Physically, this assumption means that the width of the actuator response is larger than the width of the actuator zone, i.e., the responses of the neighboring CD actuators overlap, which is often the case for CD actuator systems.

5.1 Primary frequency subband

In our analysis, we have subdivided the frequency bands of the high- resolution profiles into m_a frequency subbands in accordance with (22). As the actuator frequency response is small for higher frequencies, we can analyze the results by taking into account only two terms - two frequency ranges - in the sums (28)–(29), and (36)–(37). This terms correspond to the first and last of the m_a subbands. To make this idea clearer, Figure 2 shows a typical appearance for spectra of the initial high-resolution actuator profile, actuator response, and actuator setpoint profile. In accordance with(19), all real profile spectra that we consider are symmetrical with respect to the middle point. Thus, the high-resolution profiles in question are relatively large in the first subband, and, symmetrically, in the last subbands range, while being small in other frequency ranges. In particular, this is valid for the frequency response $\tilde{b}$ of the CD actuator.

To make the below analysis more transparent, let us convert to a physically meaningful frequency notation in such analysis. A discrete Fourier transform of a high-resolution profile p can be considered as an approximation for the Fourier transform of a continuos profile sampled with the scanner resolution. Let us choose the actuator spacing as a unit for the description of the CD coordinate of the profiles. Then, the CD coordinate of the actuator j will be $j-1$, and the CD coordinate of the high-resolution sample k will be $(k-1)/m_a$. Accordingly, instead of (18) and (20), we will consider the following notation

$$\tilde{p}[\nu] = \sum_{l=1}^{m} e^{i2\pi\nu/m_a} p_l \,, \qquad \tilde{p}_k = \tilde{p}[\nu = (k-1)/n_a] \,, \tag{38}$$

$$\tilde{u}[\nu] = \sum_{l=1}^{n_a} e^{i2\pi\nu} u_l \,, \qquad \tilde{u}_k = \tilde{u}[\nu = (k-1)/n_a] \,, \tag{39}$$

where ν is the inverse wavelength of a complex exponent measured in the actuator spacing units.

In the notation of (38), (39), the Nyquist frequency of the actuator system corresponds to $\nu = 1/2$. The symmetry property (19) of the spectra can be written in the form

$$\tilde{p}[\nu] = \tilde{p}^*[m_a - \nu], \qquad \tilde{u}[\nu] = \tilde{u}^*[1-\nu],$$

while transition to a different frequency range in (22) corresponds to changing ν by an integer number. We will further assume that $0 \le \nu \le 1$ and denote $\tilde{p}^j[\nu] = \tilde{p}[j-1+\nu]$. Then, $\tilde{p}^{m_a}[m_a - \nu] = \tilde{p}^*[1-\nu]$.

5.2 Optimal multivariable controller

To make the following analysis more transparent, it is performed using the physically meaningful frequency notation. By using the notation of (38), (39), we can estimate the spectra of the minimum variance actuator and error profile (12)– (13) for $0 \le \nu \le 1$ from (28)–(29) as

$$\tilde{u}_*[\nu] = \frac{\tilde{b}[\nu]\tilde{p}[\nu] + \tilde{b}[1-\nu]\tilde{p}^*[1-\nu]}{\tilde{b}[\nu]^2 + \tilde{b}[1-\nu]^2} \tag{40}$$

$$\tilde{e}_*[\nu] = \tilde{b}[1-\nu]\frac{\tilde{b}[1-\nu]\tilde{p}[\nu] - \tilde{b}[\nu]\tilde{p}^*[1-\nu]}{\tilde{b}[\nu]^2 + \tilde{b}[1-\nu]^2} \tag{41}$$

One can see from (40), (41) that the minimum variance solution has a nonzero error $\tilde{e}_*[\nu]$ in the Nyquist frequency range (for $0 \le \nu < 1/2$), unless the actuator response spectrum $\tilde{b}[\nu]$ is zero beyond this range (for $1/2 \le \nu \le 1$).

First, let us consider the case, where the actuator response spectrum $|\tilde{b}[\nu]|$ decays fast and is close to zero for $\nu > \nu_0$, where $\nu_0 < 1/2$. This is the case of actuator response being much wider than the actuator spacing. In such case, the denominator in (40) is close to zero in the frequency interval $\nu_0 < \nu < 1 - \nu_0$. Therefore, the spectrum of the minimum-variance actuator profile input $|\tilde{u}_*[\nu]|$ will be large in the same interval, which will be observed as actuator picketing. A possible control strategy to overcome the picketing is to add some penalty for the control by using a regularized performance index (14). This approach adds a small positive constant to the

denominator in (40), (41). The regularization would improve the actuator profile appearance, but may increase the error for high frequency ($\nu > \nu_0$) components of the measured profile, which are, in this case, poorly controllable.

Now let us consider the case, where the actuator response spectrum $\tilde{b}[\nu]$ is significant over a frequency interval stretching beyond the Nyquist frequency $\nu = 1/2$. This is the case of a relatively narrow actuator response. Let us study the spectral content of the residual error profile $\tilde{e}_*[\nu]$ at frequencies $\nu = 1/2$ and $\nu = 1$.

For the Nyquist frequency $\nu = 1/2$, we obtain from (41)

$$\tilde{e}_*[1/2] \;\; = \;\; i \; \mathrm{Imag} \; \tilde{p}[1/2] \, , \tag{42}$$

where Imag denotes an imaginary part of a complex number. The imaginary part of $\tilde{p}[1/2]$ corresponds to the profile component at the Nyquist frequency, which is out of phase with the CD actuator system and, therefore, is not controllable using this actuator system. Notably, the error (42) at the Nyquist frequency does not depend on the actuator response shape.

For the frequency $\nu = 1$, the wavelength is equal to the actuator spacing. Since the spectral response of the actuator decays for high frequencies, we will assume that $|\tilde{b}[1]| \ll |\tilde{b}[0]|$. By neglecting $\tilde{b}[1]$ in the denominator of (41), we obtain

$$\tilde{e}_*[1] \;\; \approx \;\; \tilde{p}[1] - \tilde{p}^*[0] \frac{\tilde{b}[1]}{\tilde{b}^*[0]} \, , \tag{43}$$

The first term in (43) is the uncontrollable initial spectral component of the profile at the considered frequency. The second component shows an aliased influence of the zero-frequency component of the initial error profile and it might mean a control-caused increase of the error. Though this second component is multiplied by a small value $\tilde{b}[1]/\tilde{b}^*[0]$, the initial zero-frequency error $\tilde{p}[0]$ (initial mean error) is usually much larger than the higher frequency components of the error. Thus, the error profile might exhibit a significant error at the frequency $\nu = 1$, if the ratio $|\tilde{b}[1]|/|\tilde{b}[0]|$ is not small enough. Such an error concentrated around a specific frequency will appear as periodic streaks in the error profile. These streaks are related to such design parameters of the CD actuator system as response shape and actuator spacing. They cannot be improved by the CD control, since we already consider the minimum variance control here.

On the other hand, such streaks can be potentially changed by changing paper machine or actuator design parameters which influence CD response width and shape.

5.3 Mapped CD control

Let us now analyze the frequency domain expressions (28)–(29) for the mapped CD control and high-resolution profile error in the same way as we have just done for the minimum variance control. We will use the frequency notation introduced in this section and consider only the first and last frequency subbands. We will assume that the mapping window h_k is symmetric and, therefore, $\tilde{h}[\nu]$ is always real. Similarly to (40)–(41), we obtain

$$\tilde{u}_M[\nu] = \frac{\tilde{h}[\nu]\tilde{p}[\nu] + \tilde{h}[1-\nu]\tilde{p}^*[1-\nu]}{\tilde{h}[\nu]\tilde{b}[\nu]| + \tilde{h}[1-\nu]\tilde{b}[1-\nu]} \tag{44}$$

$$\tilde{e}_M[\nu] = \tilde{h}[1-\nu]\frac{\tilde{h}[1-\nu]\tilde{p}[\nu] - \tilde{h}[\nu]\tilde{p}^*[1-\nu]}{\tilde{h}[\nu]\tilde{b}[\nu]| + \tilde{h}[1-\nu]\tilde{b}[1-\nu]} \tag{45}$$

Let us consider the case, where the actuator response spectrum $|\tilde{b}[\nu]|$ is significant over a frequency interval prolonging beyond the Nyquist frequency $\nu = 1/2$. This is the most interesting case of a relatively narrow actuator response. We will study the spectral content of the residual error profile $|\tilde{e}_M[\nu]|$ at frequencies $\nu = 1/2$, $\nu = 1$, and around $\nu = 1/2$.

For the Nyquist frequency $\nu = 1/2$, we immediately obtain that, irrespectively of the mapping window shape, the error is always the same as in (43)

$$\tilde{e}_M[1/2] = i\text{Imag}\,\tilde{p}[1/2]$$

For the frequency $\nu = 1$ defined by the actuator spacing, we will assume that $|\tilde{b}[1]| \ll |\tilde{b}[0]|$ and $|\tilde{h}[1]| \ll |\tilde{h}[0]|$. By neglecting $\tilde{b}[1]\tilde{h}[1]$ in the denominator of (45), we obtain the result coinciding with (43)

$$\tilde{e}_M[\nu] \approx \tilde{p}[1] - \tilde{p}^*[0]\frac{\tilde{b}[1]}{\tilde{b}^*[0]}\,,$$

Thus, under mild assumptions on the mapping window shape, the mapped controller error for $\nu = 1/2$ and $\nu = 1$ does not depend on this shape and coincides with the error for minimum variance controller. Therefore, the above discussion of the similar results obtained for the minimum variance controller is applicable to the results for the mapped controller as well.

A minimum-variance and a mapped controller will however give different results for frequencies around the Nyquist frequency $\nu = 1/2$. Let us study comparative error for these two controllers. Though each of the errors (41) and (45) depends on the initial error profile $\tilde{p}$, their ratio depends only on the actuator response and mapping window shapes. By dividing (45) and (41) we obtain an increase of the mapped controller error relative to the minimum variance controller.

$$\frac{\tilde{e}_M[\nu]}{\tilde{e}_*[\nu]} = \left(1 + \left|\frac{\tilde{b}[\nu]}{\tilde{b}[1-\nu]}\right|^2\right)\left(1 + \frac{\tilde{\phi}[\nu]}{\tilde{\phi}[1-\nu]}\left|\frac{\tilde{b}[\nu]}{\tilde{b}[1-\nu]}\right|^2\right)^{-1}, \tag{46}$$

where $\tilde{\phi}[\nu] = \tilde{h}[\nu]/\tilde{b}[\nu]$ is the ratio of the mapping window spectrum to the actuator response spectrum. In particular, one can immediately see from (45) that for $\nu = 1/2$ the ratio of the errors is always unit. The estimate (45) gives a qualitative understanding of the CD controller error around the Nyquist frequency. This estimate is accurate for $\tilde{b}[\nu]$ being not exceedingly small, otherwise the aliased influence of higher harmonics can be comparable to contribution of the two harmonics considered.

Let us analyze (46) in more detail. Currently, in many industrial CD control system, the mapping window is significantly narrower than the actuator response. Therefore, the spectral width of the mapping window is larger than the spectral width of the actuator response - one can call such situation "underfiltering". This means that the actuator response spectrum $\tilde{b}[\nu]$ decays steeper than the mapping window spectrum $\tilde{h}[\nu]$ and, thus, their ratio $\tilde{\phi}[\nu]$ grows with the frequency. Hence, $\tilde{\phi}[\nu]/\tilde{\phi}[1-\nu] < 1$ for $\nu < 1/2$, and the ratio (46) exceeds 1 below the Nyquist frequency, while being lower than 1 above this frequency. A noticeable error spectrum just below the Nyquist frequency is observed in MDI practice of the CD control. A reduction of the error spectrum below the Nyquist frequency was observed in tests of a minimum variance controller [13].

To the contrary, overfiltering (an application of an overly wide antialiasing window) will result in decaying ratio $\tilde{\phi}[\nu]$. Therefore, the mapped controller would have a larger error just above the Nyquist frequency.

5.4 Possible reasons for streaks

Based on the above discussion, the streaks - periodic disturbances of the high resolution profile - can be caused by the following reasons.

First, streaks might appear at the actuator frequency (twice the Nyquist frequency). The spectral power of such streaks is given by (43). Such streaks might become noticeable if the actuator response is narrow compared to the actuator spacing. This corresponds to the spectrum of the actuator response being wide, i.e., still significantly above zero at twice the Nyquist frequency. The relative width of the response is related to the design of an actuator system and could be possibly improved by reducing the actuator spacing.

Second, the relatively large spectral power of the profile variations below the Nyquist frequency could be caused by the usual practice of underfiltering in the mapped controller. Underfiltering means that the actuator response is wider than the joint width of the actuator zone and the 'antialiasing' filter window. In this case, the profile spreads can be reduced by using a wider antialiasing window or employing a minimum variance controller (which corresponds to the window shape coinciding with the actuator response shape).

Third, streaks can be caused by presence of uncontrollable components in the initial profile at the Nyquist frequency and out of phase with the actuators. Such streaks are process related and cannot be dealt with by control tuning or signal processing. It is possible to make a conclusion about controllability of the streaks by performing a model-based analysis. Software tools for such analysis will become available in the next generation of advanced CD control systems.

6 Paper Machine Data Example

This section applies the analysis tools developed in this paper to a field installation of a CD control system for a paper machine, where streaks are observed. The data below was obtained at a North American paper mill.

Before discussing the analysis results, consider the controlled process, which is shown in Figure 1. In a Fourdrinier paper machine where the data was collected, similar to this in

Figure 1, the liquid paper stock (pulp) is extruded from the *headbox* onto the top of the horizontal surface of the moving *wire* as illustrated in Figure 3. The wire is a machine-wide band of a fine metal or plastic mesh made into a closed loop. The water in the stock drains through the wire while the wood fibers are retained on the top of the wire. At the end of the wire, the solidified stock enters the next stage of the paper making process.

The paper machine uses slice lip CD actuators for the paper weight control. The slice lip is a metal bar covering one side of the gap in the headbox, where the stock is extruded onto the wire. The slice lip actuators are electric drives that pull the slice lip down or push it up the at different points in the CD. The actuator action bends the slice lip, respectively increasing or decreasing the extrusion gap where the actuator is attached. The resulting local change in the stock flow results in a localized change of the produced paper weight.

The paper machine, where the data was collected, has 66 slice lip actuators uniformly distributed in CD direction across the headbox with of 8.28 m (330 in). The produced paper is further trimmed to about 7 m width. The machine speed is 16.3 m/s (37 mph). It produced light coated paper grade with the weight of 32.6 g/m^2 (22 lbs/3300 ft^2). The paper weight profile is measured by a scanning gauge located at the dry end of the paper machine just before the coater, 1050 m of paper downstream from the slice lip. The scanner supplies a high-resolution profile with a 22.8 mm databox resolution every 22 seconds. This profile is mapped to actuator-resolution control error profile as described in Section 2 of the paper.

The problem streaks do not show up on the control error profile and, thus, are not controllable with the mapped CD control system. The data used for the analysis included the steady-state high-resolution error profile obtained for the working CD control system. This profile corresponds to good compensation of the control error profile and is shown in the upper plot in Figure 5.

In order to verify the system alignment and identify a multivariable model of the CD control, an identification experiment was performed on the paper machine. In the experiment, the CD actuators were put off feedback control. After collecting 20 scans of the baseline data with fixed actuator setpoints, three actuators were stepped up (bumped) to new setpoints and 20 more scans were collected after the process reached new steady state. By finding average baseline

and bump profiles and subtracting them the differential response profile was obtained. The differential response profile together with the actuator bump profile are shown in Figure 4. The data in Figure 4 was used to identify a parametric model of the process response and mapping using the tools described in [8, 9, 10].

The identified parametric model for the response shape function b (6) has the form

$$b(k) = ge^{-ak^2/w^2} \cos(\pi x/w), \tag{47}$$

where the response width is $w = 8.85$ databoxes, the attenuation parameter is $a = 1.5$. The response gain g in (47) is defined for the actuator profile (slice lip opening variation) measured in μm and the paper weight measured in g/m^2. The identified gain was $g = 3.71$ g/m^2 per μm. The response profile modeled in accordance with (47) is shown in Figure 4 as a smooth curve in the upper plot.

The identification results allow us to compute the gain matrix G in (4). The system in question does not use an antialiasing filter, and the mapping window h in (10) is a rectangular averaging window. In order to validate the obtained matrix model, the minimal achievable error of the mapped controller was computed from the condition of the zero control error profile. This error is shown in the middle plot of Figure 5, while the top plot shows the experimentally obtained steady-state error profile. The achieved quality of the model prediction indicates that the identified model is sufficiently accurate.

The lowest plot in Figure 5 illustrates the error profile obtained for a multivariable controller in accordance with (13). Though the results for the multivariable controller are slightly better than for the mapped controller used presently, a significant part of the streaks remains present in the profile. Since the multivariable compensation provides *minimal* possible variation of the error profile for the given response shape, one has to conclude that the streaks are not controllable and cannot be improved by the control tuning. It is believed that the streaks present in this case are linked to a mechanical or flow related process problem.

The spectral characteristics of the mapping window and the actuator response shown in the upper plot of Figure 6 demonstrate that the mapped controller spectral window is much wider than for the optimal multivariable controller. Therefore, the mapped controller 'underfilters' the error profile. As discussed in Subsection 4.2, such underfiltering should result in an in-

creased variation of the mapped controller in the frequency range below the Nyquist frequency. To illustrate this point, the lower plot in Figure 6 shows spectra for the initial profile, error profile for mapped controller, and error profile for the mapped controller. As expected, the multivariable controller provides a smaller error below the Nyquist frequency, while having a slightly larger error above this frequency. The peak at $\nu \approx 0.53$, which corresponds to the uncompensated streaks, comes from the initial profile and is believed to be process-related.

7 Conclusions

The analysis performed in this paper has shown that the performance of a mapped controller or optimal cross-direction controller is limited by the spatial response frequency characteristics. The performance of either a mapped controller or an optimal multivariable controller has been shown to be identical if the mapping window equals the spatial response shape. Narrow streaks close to Nyquist frequency, defined by twice the actuator spacing cannot generally be corrected with CD control changes. They are often found to be process-related and must be eliminated at the source.

References

[1] Aidun, C.K. "A fundamental opportunity to improve paper forming," *TAPPI Journal*, Vol. 79, No. 6, 1996, pp. 55–60.

[2] Bergh, L.G. and MacGregor, J.F. "Spatial control of sheet and film forming processes," *Canadian J. of Chem. Eng.*, Vol. 65, February 1987, pp. 148–155.

[3] Boyle, T.J. "Practical algorithms for cross-directional control," *Canadian J. of Chem. Eng.*, Vol. 35, 1977, pp. 457–461.

[4] Chen, S.-C. and Wilhelm R.G. "Optimal control of cross-machine direction web profile with constraints on control effort," *American Control Conf.*, June 1986, pp. 1409–1415.

[5] Duncan, S.R. "The design of robust cross-directional control systems for paper making," *American Control Conf.*, Seattle, WA, June 1995, pp. 1800–1805.

[6] Duncan, S.R., and Bryant, G.F. "The spatial controllability of cross-directional control systems for web processes," *Automatica*, Vol. 33, No. 2, 1997, pp. 139-153.

[7] Gantmacher, F.R. *The Theory of Matrices.* Chelsea Pub., New York, 1959.

[8] Gorinevsky, D. and Heaven, M. "Automated identification of actuator mapping in cross-directional control of paper machine," *American Control Conf.*, Albuquerque, NM, June 1997, pp. 3400-3404

[9] Gorinevsky, D., Heaven, M., et al. (1997) "Advanced on-line automated identification tool for mapped and multivariable cross-directional control," *XIV IMEKO World Congress/CD Symposium*, Finland, June 1997. pp. 162-167.

[10] Gorinevsky, D., Heaven, M., et al. "New algorithms for intelligent identification of paper alignment and nonlinear shrinkage," *Control Systems '96*, Halifax, N.S., Canada, April 1996, pp. 41–47, 1956.

[11] Halouskova, A., Karny, M., and Nagy, I. "Adaptive cross-direction control of paper basis weight," *Automatica*, vol. 29, no. 2, 1993, pp. 425–429.

[12] Heath, W.P. "Orthogonal functions for cross-directional control of web forming," *Automatica*, vol. 32, no. 2, 1996, pp. 183–198.

[13] Heaven, E.M., et al. "Recent advances in cross-machine profile control," *IEEE Control Systems Magazine*, October 1994, pp. 36–46.

[14] Heaven, E.M., et al. "Application of system identification to paper machine model development and simulation," *Control Systems '92*, Whistler, B.C., Canada, September 1992, pp. 271–278.

[15] Laughlin, D.L., Morari, M., and Braatz, R.D. "Robust performance of cross-directional control systems for web processes," *Automatica*, Vol. 29, No. 6, 1993, pp. 1395–1410.

[16] Lee, C.A. "Streaks on paper machines as related to a stable spiral flow in the inlet," *Pulp and Paper Magazine of Canada*, Vol. 57, No. 3, The convention issue, pp. 176–182.

[17] McFarlin, D.A. "Control of cross-machine sheet properties on paper machines," *Process Control Symposium*, 1983, pp. 49–54.

[18] Offerhaus, D.H. "The challenge, lapping a headbox apron flow," *CPPA Technical Paper* presented at Control Systems '92, Whistler, B.C., September 1992

[19] Offerhaus, D.H. "Continuing the challenge, "Blueprinting" a headbox," *Pulp and Paper Canada*, Vol. 97, No. 6, pp. T216-T222, 1996.

[20] Oppenheimer, A.V., Schafer, R.W. *Discrete-time Signal Processing*. Prentice Hall, Englewood Cliffs, N.J., 1989

[21] Rawlings, J.B. and Chien, I-L. "Gage Control of Film and Sheet-Forming Processes," *AIChE J.*, Vol. 42, No. 3, 1996, pp. 753–766.

[22] Sanford, C.L. "Characteristics of flow from a two-dimensional nozzle with a multiple-tube inlet," *TAPPI Engineering Preprints*, pp. 159–164, 1976

[23] Skogestad, S. and Postlethwaite, I. *Multivariable Feedback Control*, Wiley, Chichester, 1996.

[24] Stewart, G.E., Gorinevsky, D.M., and Dumont, G.A. "Robust GMV cross directional control of paper machines," *American Control Conf.*, Philadelphia, PA, USA, June 1998, pp. 3002–3007.

[25] Tikhonov, A.N., and Arsenin, V.Ya. *Solutions of Ill-Posed Problems.* Halsted Press, Washington, 1977.

[26] Vaidyanathan, P.P. *Multirate Systems and Filter Banks*, Prentice Hall, Englewood Cliffs, 1993.

[27] Wilhelm, R.G. and Fjeld, M. "Control algorithms for cross-directional control: The state of the art," *5th IFAC PRP Conf.*, Antwerp, Belgium, 1983, pp. 139–150.

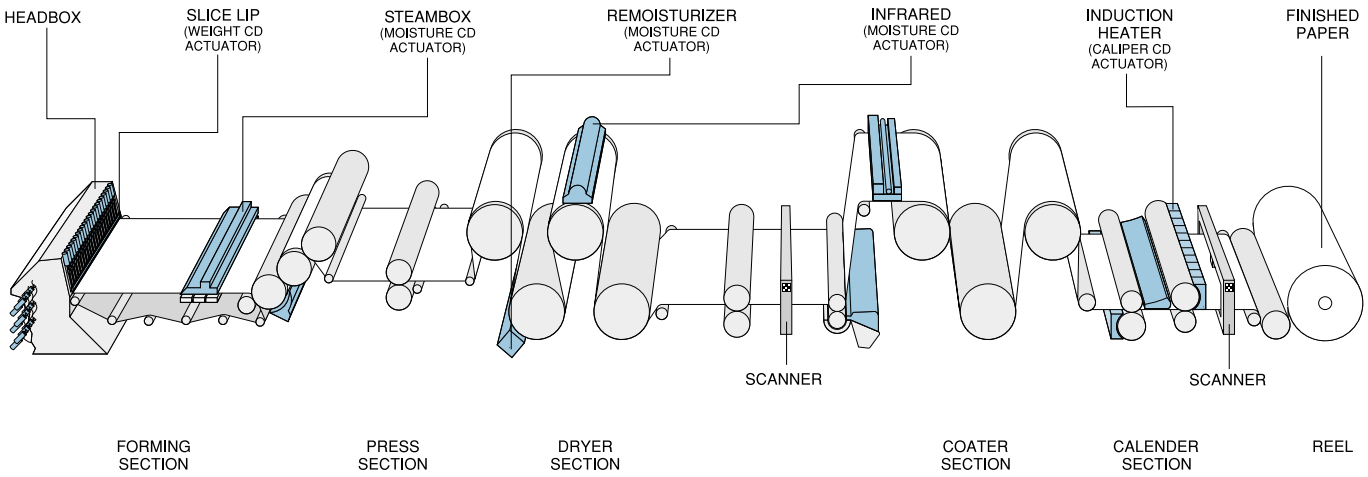

Figure 1: Paper Machine.

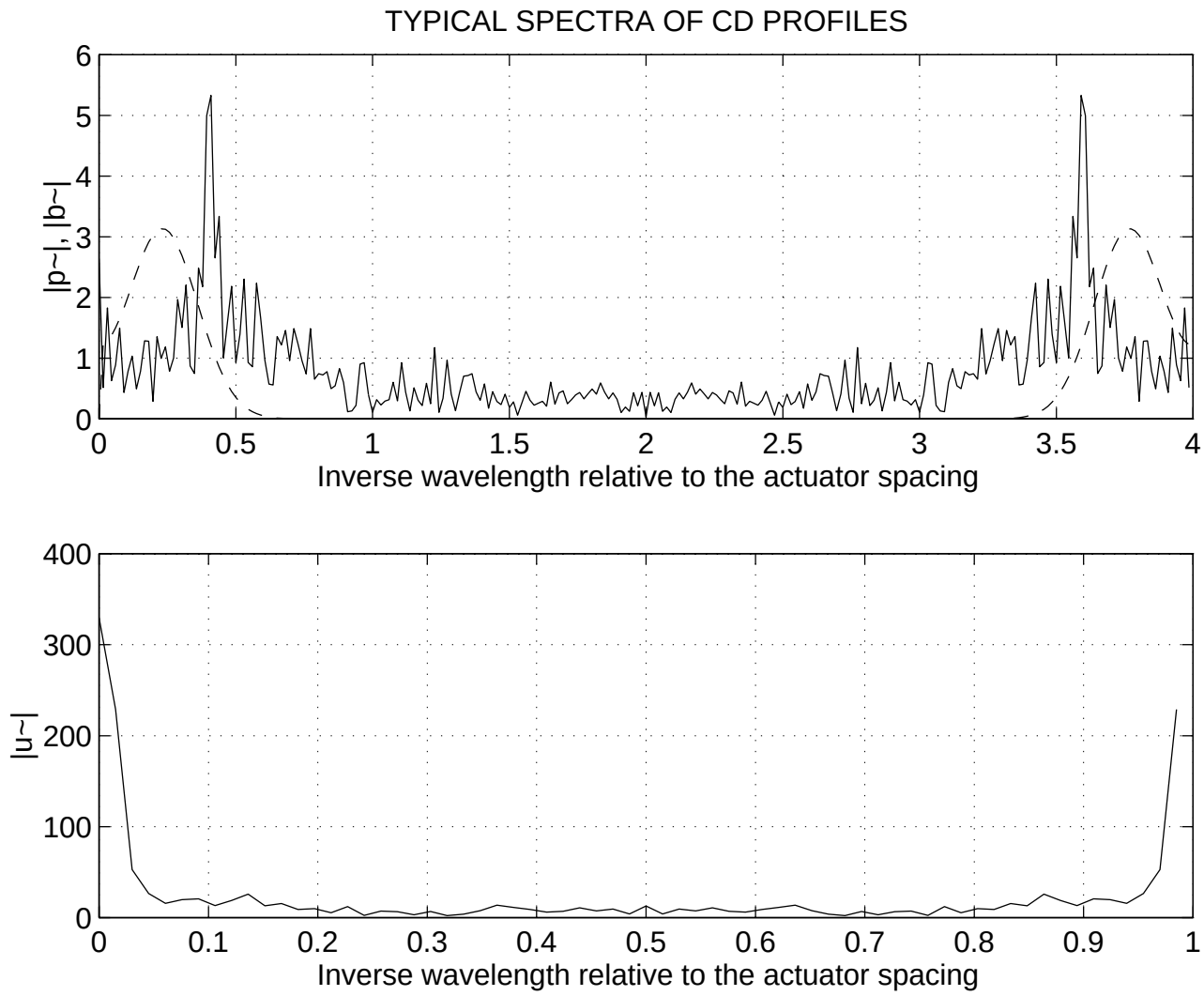

Figure 2: The upper plot shows typical spectrum $|\tilde{p}|$ of the initial high-resolution profile (dashed) and actuator response $|\tilde{b}|$ (solid). The lower plot shows typical spectrum of the actuator setpoint profile $\tilde{u}$.

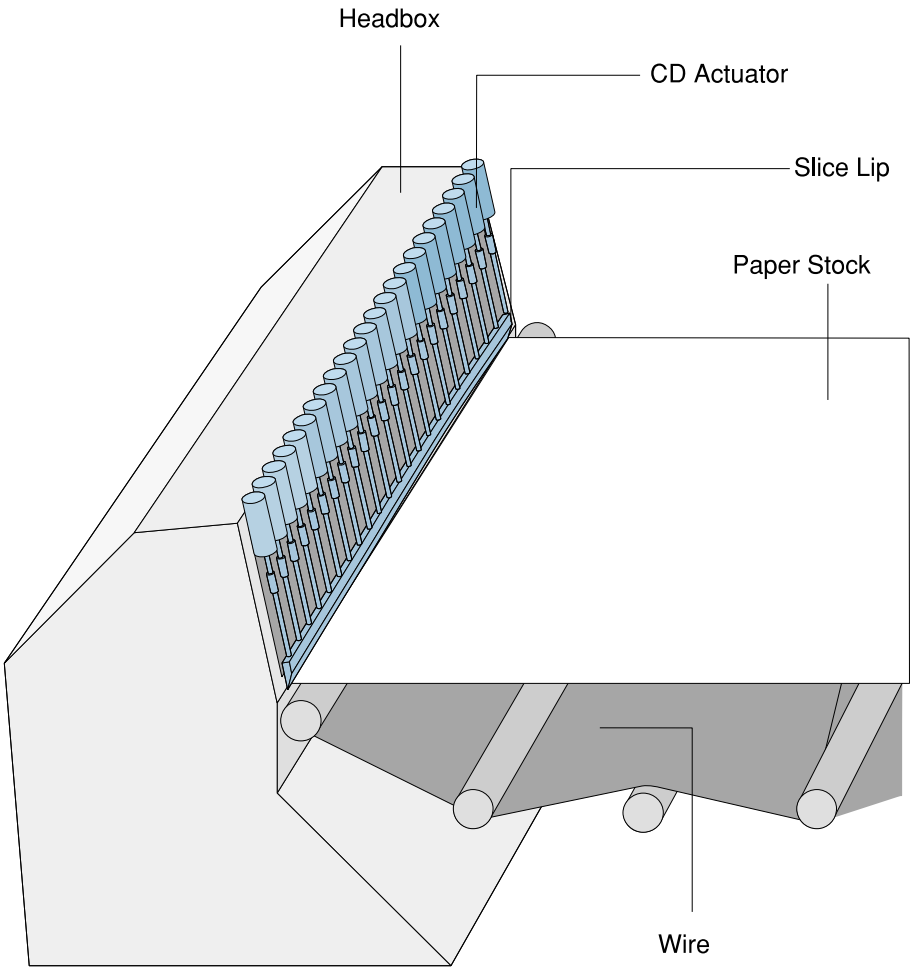

Figure 3: Paper machine headbox

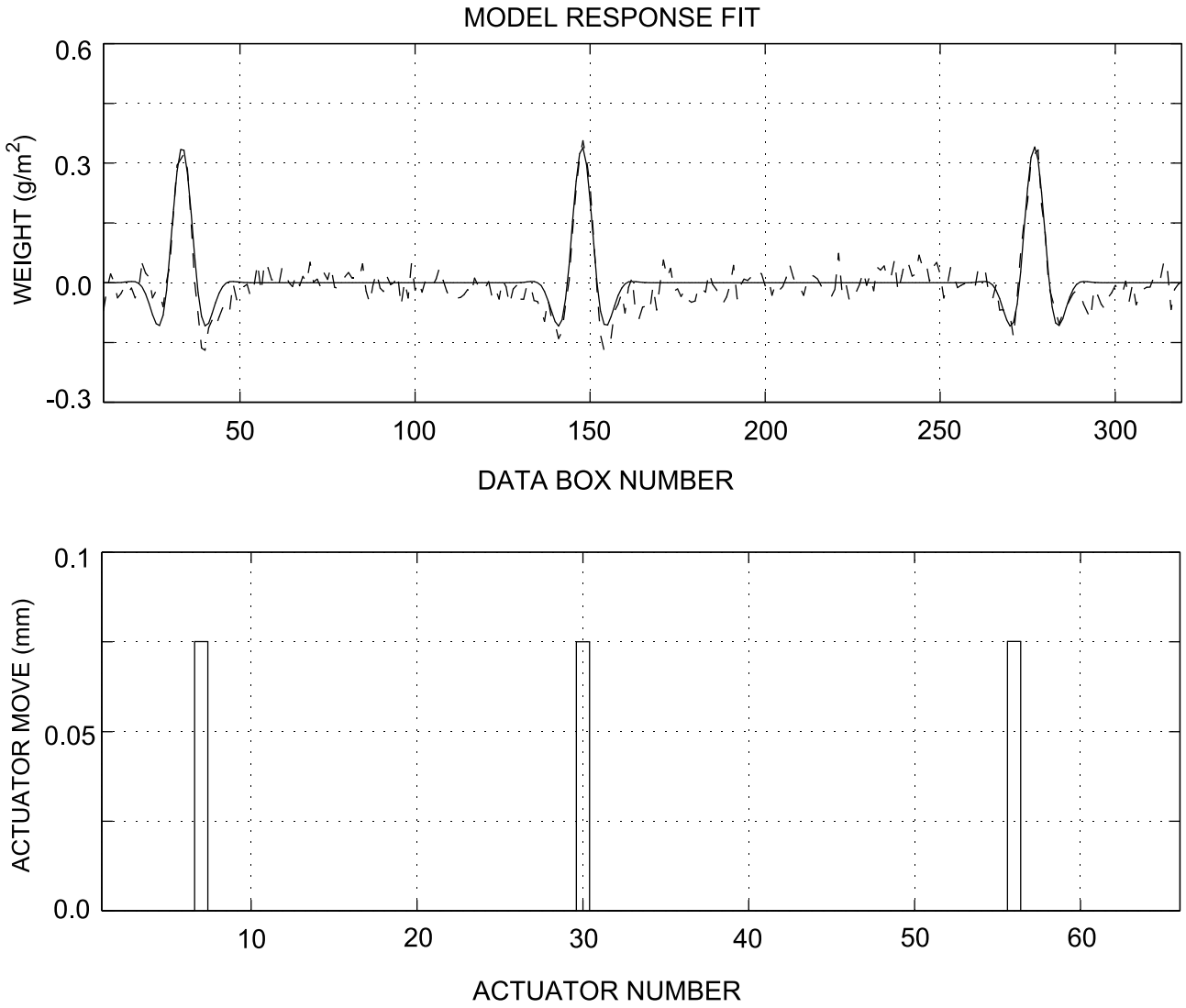

Figure 4: Multivariable model identification for a paper mill data. The upper plot: the model response identified from the data (solid) and the averaged incremental steady-state measured response of the CD process (dashed). The lower plot: the incremental actuator profile applied in the step response test.

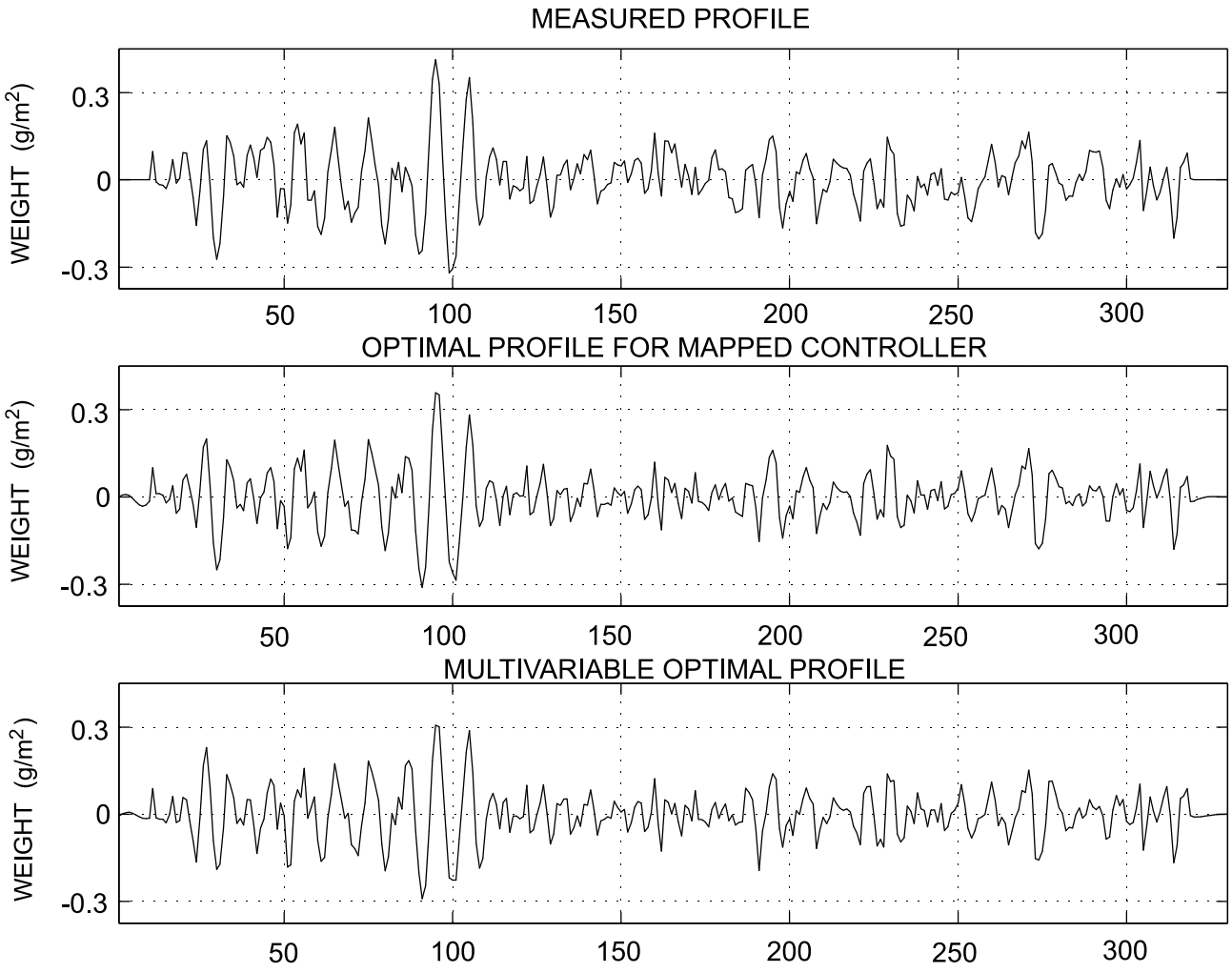

Figure 5: Plots from top to bottom: 1) the experimentally obtained steady state error profile; 2) the theoretically optimal error profile for a mapped controller; 3) the multivariable optimal error profile

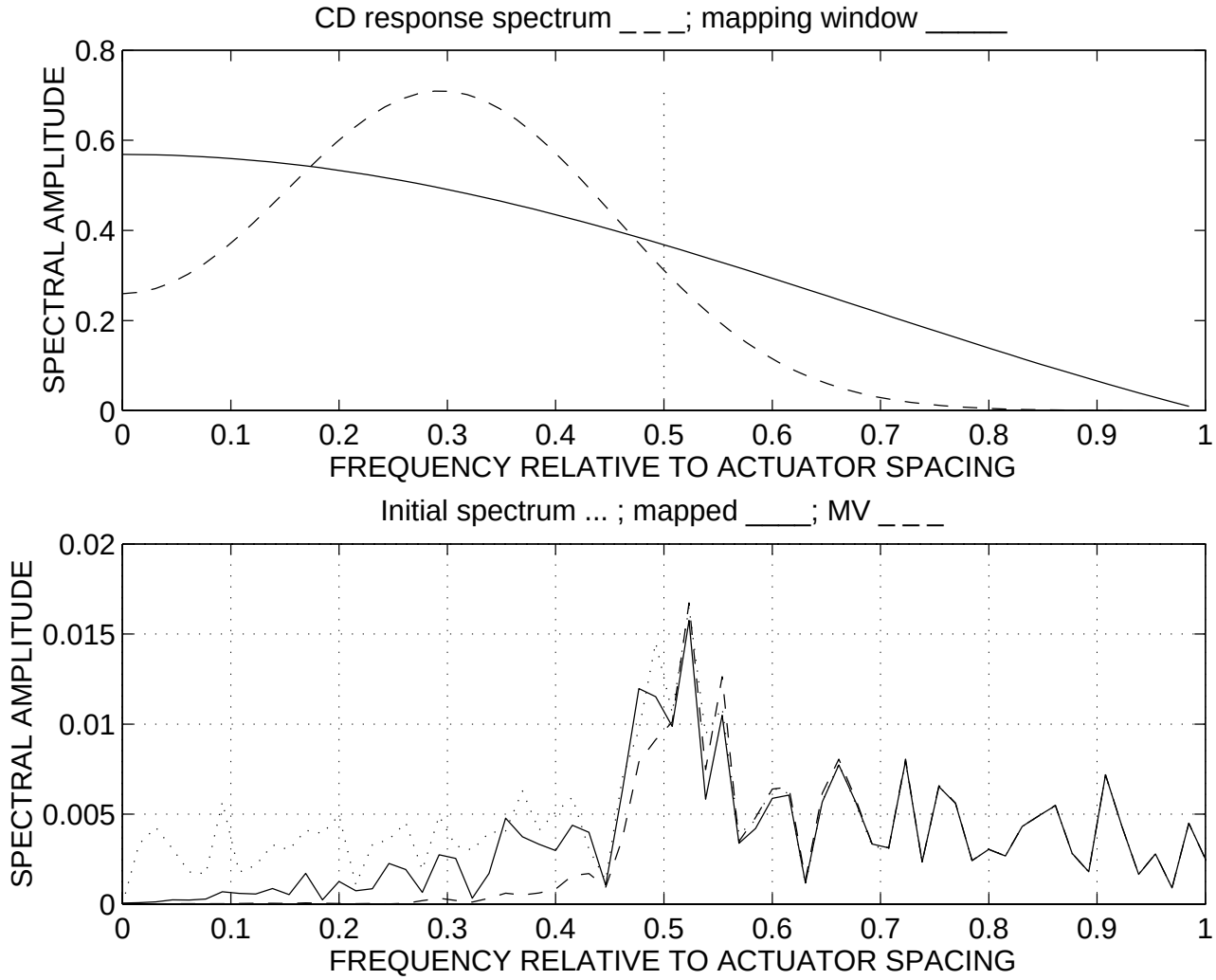

Figure 6: Upper plot: CD spectrum of the actuator response - dashed; spectrum of the mapping window - solid. Lower plot: Spectral content of error profiles. Mapped controller - solid; multivariable controller - dashed; initial error profile - dotted.